AN EXPERIMENTAL INVESTIGATION INTO THE EFFECTS INITIAL CONDITIONS AND WATER ON DECK HAVE ON A THREE DEGREE OF FREEDOM CAPSIZE MODEL

Michael S. Obar, Young-Woo Lee, and Armin W. Troesch
Department of Naval Architecture and Marine Engineering
University of Michigan, Ann Arbor, Michigan, USA 48109-2145
e-mail: mobar@engin.umich.edu, ywl@engin.umich.edu, troesch@engin.umich.edu

SUMMARY

This paper presents the preliminary results of a three degree-of-freedom (3DOF) vessel capsize experiment and analysis conducted at the University of Michigan Marine Hydrodynamics Lab during the late spring of 2001. A box barge with minimal freeboard was placed in a beam sea and was excited at a super-harmonic three times its roll natural period. The motion of this vessel was captured using a locally developed infrared motion capture system. The video was stored electronically and analyzed using the computer program MATLAB©. The vessel was heeled at varying initial roll angles and released at twelve different locations in the wave train, each corresponding to a quarter of the wave excitation period. This was done to induce various initial conditions at a defined reference point (t_o). The definition of a safe basin of initial conditions and the effects water on deck has on this safe basin will be discussed.

1 INTRODUCTION

The fishing industry has, throughout history, been regarded as an extremely hazardous occupation. Even without the threat of a vessel capsizing, the chances of surviving a long career as a commercial fisherman are not very favourable.

Now, as the quantities of fish and number of species dwindle, and the regulations continue to become more stringent, fishermen must push the capabilities of their vessels to the brink, past which there may be no return. As captains push their vessels with overloading and tempt mother nature with trips into rougher weather, the need to better understand the dynamic nature of a vessels capsize becomes of great importance.

The phenomena of vessel capsize is an extremely complicated dynamic event. Environmental forces, hull design, and vessel loading are just of few of the hundreds of factors that affect the safety and stability of the vessel. In order to better understand this phenomena, the affect of an initial roll angle and velocity pair, coupled with water on deck will be analyzed in this paper.

Roll dynamics are best described by a nonlinear system whose response and eventual state (capsize or non-capsize) is frequently dependent upon initial conditions [1]. Additionally, water on deck produces variable loads that may have large impact on the motions. While there has been significant work investigating water on deck dynamics, e.g. [2]-[11], little attention has been given to the initial state of the vessel subject to these variable loads. Based on the work of Soliman and Thompson [1], an experiment was devised to investigate the affects of varying initial roll angle and roll velocity in a 3DOF system vice a 1DOF system.

2 BARGE PARTICULARS

The model used for the primary experiments was a simple box barge constructed of plywood and coated with West Systems epoxy. See Fig. 1. The model has a Plexiglas "main deck" and an aluminium platform supported by 4 threaded rods. Mounted on the platform are two infrared lights. The length of the model was 66.0cm. The model had a draft of 18.25cm with a freeboard of 1.12cm.

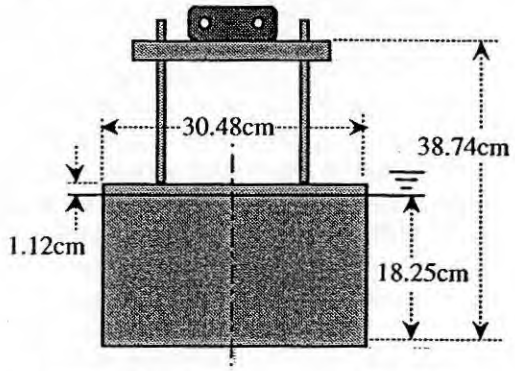

Figure 1: Sketch of barge with dimensions.

The center of gravity was adjusted to give an angle of vanishing stability, experimentally determined, of 11.4°. The deck became awash when the hull heeled approximately 5°, port or starboard. In addition to the angle of vanishing stability, the roll natural period and damping coefficients (linear and quadratic) were determined experimentally.

3 MOTION COLLECTION SYSTEM

It was critical to the analysis of this experiment to develop a system that could capture the motion of the vessel without itself affecting that motion. Two infrared LED lights were mounted on the platform of the model. A COHU 4915 High Performance Monochrome CCD Camera was mounted, in plane with the lights, with the entire test section in view. The manual iris on the camera was then closed until only the IR lights were picked up.

The rest of the test section was blacked out. The camera was connected to an ATI All-in Wonder 128 video card in a Dell PC. The movie was captured at 30 frames per second in an MPEG-1 format and saved on the hard disk for analysis at a later time. The typical movie size was around 30MB.

An intermediary program, Image Explorer Pro, was used to decompose the video into individual frames and save each frame as a JPEG image. Then, using MATLAB, each JPEG was individually loaded and scanned to find the locations of the model and indicator lights. These XY data pairs and the MATLAB workspace were then saved for future analysis. The complete analysis, including data collection, filtering of each frame to identify LED pixel position, and conversion to state six variables and three accelerations, took approximately 20 minutes per test run.

4 PRELIMINARIES

4.1 DETERMINING θ_v, THE ANGLE OF VANISHING STABILITY

A box barge was chosen as the vessel for this experiment due to its hydrostatic simplicity. Once the final weight and platform configuration was settled upon, the location of the center of gravity and θ_v was numerically determined.

The angle of vanishing stability, θ_v, was then determined experimentally. The model was placed in the test section and was manually heeled to a side. Using the motion-capture system, the model was released from the estimated location of θ_v and the motion of the vessel was captured. The vessel lolled about θ_v for several of these runs, while in others it either righted itself or capsized. After comparing the numerous runs, 11.4° was settled on as the experimental θ_v. See Fig. 2 for an example time history of the vanishing stability angle test.

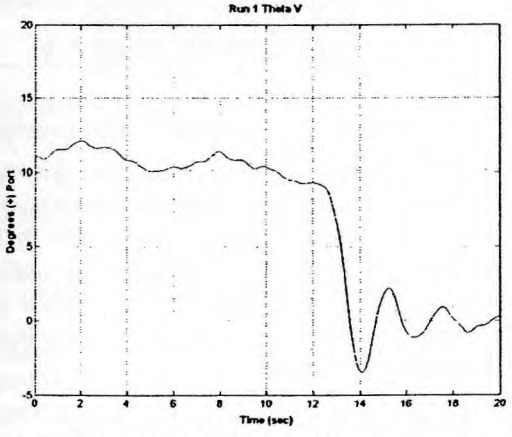

Figure 2: Vanishing Angle Determination Test

4.2 DECREMENT TESTS

Roll decrement tests were conducted in order to determine the roll natural period of the model. The model was heeled to both port and starboard and released. The motion was captured and the logarithmic decrement method was used to determine the natural period. The model was released from three heel angles, both port and starboard. The results of those tests are listed in the Table I below.

TABLE I: Decrement Test Results

Release Angle	Roll fn (Hz)	No. of Cycles
9.92	0.3669	2 analyzed
6.66	0.3605	4 analyzed
4.66	0.3639	8 analyzed
-12.96 *	0.3455 *	4 analyzed *
-10.48	0.3603	5 analyzed
-6.9	0.3645	9 analyzed
	Mean	**Standard Dev**
All 6 Runs	0.3603	0.0077
> 3 Cycles	0.3642	0.0004
> 7 Cycles	0.3589	0.0078

* Release was not clean.

Placing more emphasis on the analysis of runs with release angles less than 7° (these started with little water on deck and provided more cycles to analyze), the natural frequency was estimated to be 0.363 Hz.

4.3 DEFINITION OF t_0 AND RELEASE TIMES

In order to impart various initial conditions, the model was placed at 5 different roll angles and released at 12 different release times for each angle. Knowing the profile of the incident wave train from previous calibration runs (see the Appendix), the initial starting point, t_0,was defined as the first wave crest after the large transient, i.e. the first wave crest in the series of steady state waves. Thus all the transients that lead up to the steady state waves contributed to just the initial conditions defined at t_0. With this t_0 as a reference, it was decided to use an interval of 1/4 of a wave period between each release point and work back 3 wave periods. By releasing the model at set intervals prior to t_0, the model experienced a range of initial values for its six state variables, $(x, \dot{x})_j$ j=1...3, i.e. sway, heave, and roll motions.

4.4 AUTOMATION AND TIMING

In order to synchronize the data collection and motion collection systems, the entire process had to be automated as much as possible. Two computers were used to control the data collection and wavemaker activation. A MAC Quadra 900 running Labview 4.0 recorded the data input from the wave probes and command channels and also controlled the activation and motion of the wavemaker, while a Dell PC recorded the video.

The MAC controlled the signal output channels. The first channel was the command signal to the wavemaker amplifier. The first channel on the data collection card also captured this signal. The second output channel was a 5V low/high signal that controlled the wavemaker activation IR light. This channel was synchronised with the wavemaker command channel and signalled high as soon a command was given to the wavemaker amplifier. The second data collection channel captured this signal.

The third channel gave the control for the model release. A 5V High/Low signal was triggered once the desired release time occurred. Upon triggering, the signal activated a relay, which de-energized the DC magnets and switched on AC current to the magnets. (This helped to break the magnetic field faster.) The channel also powered the Model Release IR light and was monitored by the third data collection channel.

When the model was at the proper setting and the tank settled, the Dell video collection software started. Once a few seconds of the video had been recorded, the data collection card was triggered. It began recording the above-mentioned channels as well as the wave probe. After five seconds of data was recorded, the wavemaker command program was triggered and wave generation began.

In the post-data processing, the data time series and video was synchronized by using the hi/low channels in the data record and the lights in the video record. During the analysis of the scanned videos, the frame (accurate to the nearest 1/30 sec) where the wavemaker and models IR lights trigger, was determined thus synchronizing the video with the wave record.

5 EXPERIMENTAL SETUP AND TEST PROCEDURE

The experiments were conducted in the Gravity Wave Facility at the University of Michigan Marine Hydrodynamics Lab. The Gravity Wave Tank is 35m long, 0.75m wide, and 1.5m deep. It has a computer controlled, plunger style wavemaker. The Gravity Wave Tank also has wind generation capabilities. Although we will not be using this capability, the wind generation equipment limits the depth of the water, e.g. for a maximum wave height of 10cm, the depth of water is limited to 65cm.

For the experiments described here, the model was placed in the tank with its port side towards the wavemaker. The model was fixed in an initial position by electro-magnets suspended from the top of the tank. The release location for every run was 15.44m from the wavemaker. This position was chosen due to the location of the edge of the video frame in relation to the test section. The magnets held the model by brackets mounted on the platform. The electro-magnets were on a pivoting arm, which allowed for the vessel to be set at an initial roll angle. Once the model was released from the magnets, the pivoting arm also allowed the magnets to be swung out of the way of the platform.

The primary wave probe used to capture the wave profile of each run was mounted 8.86m down-tank from the wavemaker. This distance to the wavemaker was limited by the location of the wind generation scoop.

Four reference IR lights were mounted on the exterior of the test section glass in each corner of the video frame. See Fig. 3 for an example frame. The upper right reference light was also used as the video trigger for wavemaker activation and the lower right reference light was used as a trigger for the model release.

The two left hand reference lights were used for determining any camera twist. In order to ensure the camera always remained in the same position a MATLAB plugin allowed camera frames to be taken and imported directly into memory. This allowed for corrections to the camera position prior to every run.

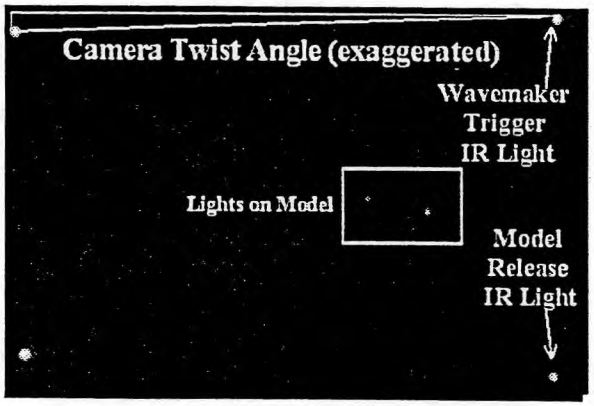

Figure 3: View of test section during run.

The testing began with the camera position verification. Several pictures were taken and compared to a reference picture. The camera was then adjusted slightly until the pictures were aligned with the reference. At the same time, the primary wave probe 40s zero was taken.

Next, the magnetic arms were set to the desired initial roll angle. The model was then placed in position and the magnets energized while the tank was allowed to settle.

After the water surface returned to a calm condition, a second set of pictures was taken. These pictures were instantly analyzed and the actual initial roll angle of the vessel determined. If needed, the magnet arms were adjusted to correct the initial angle to the desired value. A sample matrix is shown in Table A.1 of the Appendix.

Once all adjustments were concluded and the tank returned to calm water, the video capture program and the data capture program were started. After 3-5 seconds of data capture, the wavemaker was energized.

Data capture continued until either the model capsized or it left the test section, drifting out of the camera's view. The data was then saved for future analysis.

6 WAVE DETERMINATION AND ANALYSIS

6.1 WAVE DETERMINATION

The physical dimensions of the Gravity Wave Tank and the wavemaker design limited the available frequency of the waves and wave heights. Being unable to excite the vessel at or near its roll natural frequency of 0.363Hz, it was decided to excite the model at a super-harmonic of 1.089Hz, or 3 times the natural frequency.

The appropriate incident wave height was determined experimentally. Several wave runs were conducted with no artificial initial conditions imparted to the vessel. The vessel was set motionless at the release location and a test wave train was generated. Capsize or no-capsize was recorded and a second wave height was attempted. Once the smallest wave height that consistently capsized the model was identified, the height setting was then reduced.

The goal was to find the largest wave height where the vessel did not consistently capsize. That height, 2.67cm for the particular set of barge particulars and incident wave frequency described here, became the excitation wave height. The intent of this process was to determine an experimental critical wave height [1] where initial conditions imparted upon the vessel would create the likely conditions needed for capsize.

During these early tests, it was noticed that a slight longitudinal variation in the release point of the vessel (i.e. the location of the vessel relative to the wave maker), led to significant changes in the wave height needed to capsize the vessel. The variation could be a little as a few centimetres. The significance of this was noted and will be discussed in the Results/Conclusions sections.

6.2 WAVE ANALYSIS

Once the wave frequency and height was determined, 1.089Hz and 2.67cm, the repeatability of the wave generation capabilities of the tank was verified. Three wave probes were used to capture and analyze the wave profile. The primary wave probe, also used during the data collection phase, was located 8.86m down tank. A second wave probe was placed at the model release location, 15.44m down tank, and a third wave probe was placed at the end of the test section, 16.46m down tank.

6.2 (a) Wave Repeatability

Three runs were conducted with the model removed from the tank and data collection set up for the primary probe (labelled FWD Probe in the plots) and the probe at the release location (labelled Model Probe in the plots). The data collected was analyzed and plotted. Typical results are displayed in Appendix Fig. A1 indicating that wave profiles were repeatable to within 5%.

6.2 (b) Wave Reflection

Due to the finite length of the Gravity Wave Tank, it was important to ensure that the data collection and vessel capsize, occurs prior to the arrival of reflected waves off the far end of the tank. This cut-off time was determined by placing a wave probe at the end of the test section and collecting data for three separate runs.

As seen in Fig. A2, the primary crests and troughs of the steady state wave train can be identified. Once a crest and trough deviated from the mean by 1.5 standard deviations, that zero-crossing was identified as the reflection inception point. In Fig. A2, this point was approximately 62 seconds after wave maker activation. For every data run, the model either capsized or drifted out of the test section well before 60 seconds Thus wave reflection was not an issue with the experiments reported in this work.

6.2 (c) Wave Propagation

The initial transient of the wave front changes as it progresses down the tank. Three calibration runs were conducted, collecting data with the primary probe and a probe located at the release point. As the wave front changes, the excitation the model sees prior to the defined starting phase, t_o, changes as seen in Fig. A3 of the Appendix. This spatial variation of the wave envelope required the capture of the profile of the entire wave surface in the test section.

6.3 TEST SECTION WAVE PROFILE CAPTURE

Due to the fact that the model was allowed to translate down the tank during a run, determining the exact wave elevation at every point in the test section using wave probes was impractical. To capture the spatial behaviour of the wave elevation at every point in the test section, a flourscein solution was dissolved into the tank. The water surface was then illuminated with a laser sheet. Three runs were then conducted without the model in the tank and a video time history was recorded and analyzed. See Fig. 4 for an example video frame. Given the undisturbed wave profile as a function of time and space, it was possible to synchronize time and location of the desired wave crest (or trough) with the barge center of gravity, thus defining the starting reference phase or time, t_o.

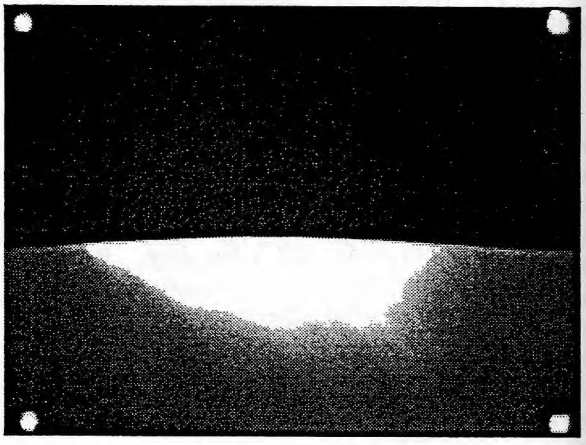

Figure 4: A view of the test section during a run. The cameras iris was opened slightly more than during a regular run.

7 MOTION ANALYSIS

The captured videos were stored in MPEG-1 format. This MPEG was separated into individual frames, e.g. Fig. 5.

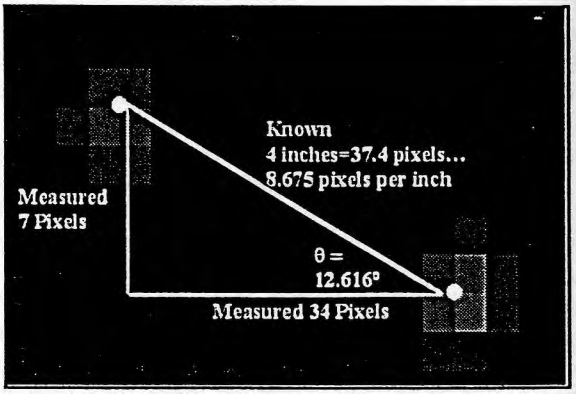

Figure 5: Blow up of the model IR lights and roll angle determination.

For each frame, a MATLAB program determined an ordered set of (x,y) data pairs representing the location of the two IR lights on the model at 1/30 sec intervals.

A third MATLAB program calculated vessel dynamics based upon the IR time series. The reference point for the model was its center of gravity. The roll, heave, and sway motions about the COG are determined using simple geometry.

Figure 6 below displays the captured motion plots. The upper plot shows roll angle vs time. All time-based position plots reference the energizing of the wavemaker at time t = 0. In Fig. 6, the model was released about 21.5 seconds after the wavemaker was energized. The model was held at a release angle of -10 degrees (starboard). The roll angle in Fig. 6 is displayed as the local roll angle. This is the roll angle relative to the wave slope at the location of the center of gravity of the model.

The first circle in the time history denotes the model release time. The second circle at approximately t=27.5sec, is the starting time of the Poincaré samples, t_0. The time interval of the Poincaré samples corresponded to the wave encounter period. The angle of vanishing stability is also marked. Note that there are many instances where the local roll angle exceeds θ_v and does not capsize.

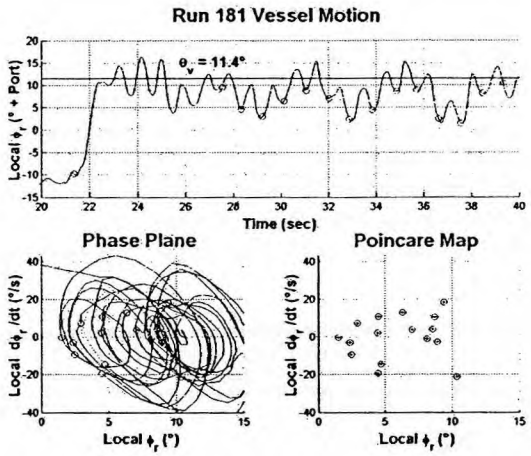

Figure 6: Vessel Non-Capsize Roll Motion (Local Roll Angle)

The motion displayed above is typical of the general trend for every non-capsize run. Runs that were initially released with a starboard roll angle, rolled down tank initially, but eventually settled in to the motion seen above. Runs that were released with a port roll angle rolled up tank immediately and also settled out to the same motion.

Figure 7 contains the same data run, only the analysis is presented with the global roll angle. The global roll angle is referenced to the earth fixed horizontal axis. The Poincaré points are sampled when each wave crest crosses the vessel's center of gravity. Using the local angle, e.g. Fig. 6, the Poincaré points map close to a "roll trough". When plotted on the global plots, e.g. Fig 7, the Poincaré points shift throughout the roll motion crests and troughs. As in Fig. 6, there are periods where the global roll angle exceeds θ_v but does not capsize.

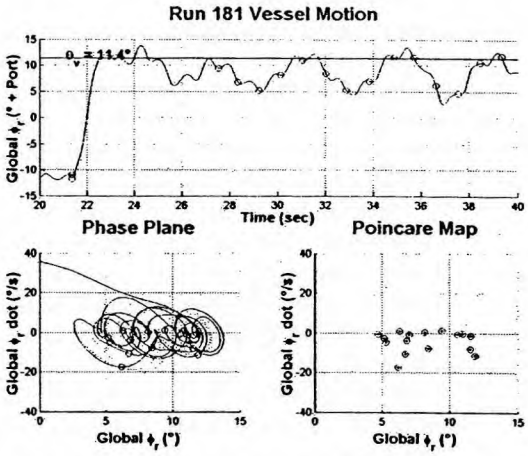

Figure 7: Vessel Non-Capsize Roll Motion (Global Roll Angle)

Figure 8 contains the motion during a capsize run. As with the non-capsize case, the motion of all the capsize situations were similar. While there may have been one or two roll-cycles prior to capsize the vessel tended to capsize and capsize quickly. For the conditions considered in this paper, all the capsize runs capsized into the waves.

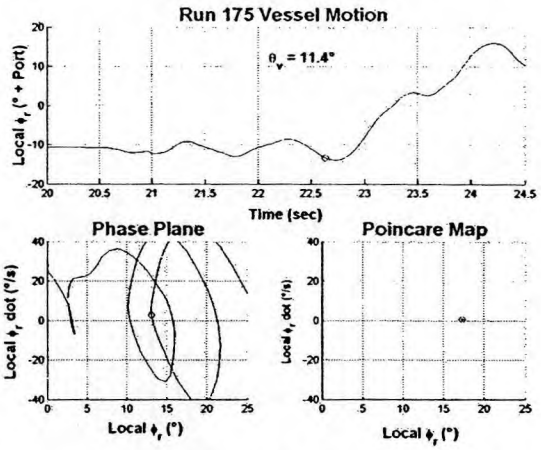

Figure 8: Vessel Capsize Roll Motion (Local Roll Angle)

8 NUMERICAL SIMULATIONS BASED ON A BLENDED HYDRODYNAMIC MODEL

To more fully understand the dynamics shown in Figs. 6-8, calculations were performed using a three degree of freedom "blended" hydrodynamic model. Various blended models have been developed approximating fully nonlinear behaviour with a combination of nonlinear and linear components [12] [13]. In this work, a quasi-nonlinear time domain simulation based on the effective gravitational field and long wave assumption [7] [14] is used. The

approximation will fully account for the effects of deck immersion in the computation of restoring forces and Froude-Krylov forces.

Briefly, the effective gravitational field is a vector combination of the earth's gravitational acceleration and the centrifugal acceleration associated with circular water particle motion. The result is a local, time varying, gravitational field perpendicular to the local water surface.

The wave contour can be prescribed by a single cosine wave of arbitrary frequency, amplitude and phase. The shape of the envelope curve of the wave profile has been adjusted to match the experimentally measured wave profile. Each wave component travels at its own phase velocity from an initial position given by its specified phase at time zero. Thus the wave elevation is completely defined at any lateral position and instant of time. At each subsequent time step, the wave contour is determined at any position of the global coordinate system, and the instantaneous displacement, center of buoyancy and local wave slope across the body are computed. From these parameters, the corresponding forces/accelerations in sway, heave and roll are computed. The accelerations are integrated at each time step to compute the velocities which are then integrated to determine the body position and orientation in sway, heave and roll.

The equations of motion, in a global, stationary axis system, are given in Eq. (1) below. The body position and orientation is given by the coordinates of the center of gravity, (x_G, y_G) and by the roll angle, φ.

$$\begin{bmatrix} m+a_{22} & 0 & a_{24} \\ 0 & m+a_{33} & 0 \\ a_{42} & 0 & I_{c.g.}+a_{44} \end{bmatrix} \begin{pmatrix} \ddot{x}_G \\ \ddot{y}_G \\ \ddot{\varphi} \end{pmatrix}$$

$$+ \begin{bmatrix} b_{22} & 0 & b_{24} \\ 0 & b_{33} & 0 \\ b_{42} & 0 & b_1 \end{bmatrix} \begin{pmatrix} \dot{x}_G \\ \dot{y}_G \\ \dot{\varphi} \end{pmatrix} + \begin{bmatrix} 0 & 0 & 0 \\ 0 & 0 & 0 \\ 0 & 0 & b_2 \end{bmatrix} \begin{pmatrix} 0 \\ 0 \\ \dot{\varphi}|\dot{\varphi}| \end{pmatrix} \qquad (1)$$

$$= \begin{pmatrix} \rho g_{e_2} \nabla + f_2^D \\ \rho g_{e_3} \nabla - mg + f_3^D \\ \rho g_e GZ \nabla + f_j^D \end{pmatrix}$$

The subscripts 2, 3 and 4 denote sway, heave and roll respectively. In the matrix, a_{ij} and b_{ij} are added mass and damping coefficients, f_j^D are diffraction forces and b_1 and b_2 are linear and nonlinear (quadratic) roll damping coefficients. Added mass, damping and wave diffraction forces are assumed constant at each wave frequency and all these coefficients are calculated using the standard linear seakeeping program, SHIPMO[15]. The nonlinear forces are associated with terms that include

g_e- the magnitude of the effective gravity,

g_{e2}, g_{e3} - the sway and heave components of the effective gravity in global axis coordinates,

b_2 - the quadratic roll damping [15],

∇ - the time dependent volume of the hull, including the occurrences of deck immersion or bottom emersion, and

GZ - the time dependent roll righting arm, referenced in the local wave slope/body coordinates.

With this model, the complex dynamic responses of the box barge with a low freeboard floating in regular beam waves can be investigated. Note that the blended model given in Eq. (1) does not include the real-life effects associated with the dynamics of water on deck such as fluid sloshing and water egress.

For the simulations presented in this paper, initial conditions for the other state variables, heave and sway displacements and velocities, were set equal to zero. This is not the case for the experiments and may be a possible explanation for any differences between simulated and experimentally measured capsize boundaries.

9 RESULTS

One hundred and eighty experimental runs were conducted. Three initial-condition sampling points were chosen, t_{o1}, t_{o2}, and t_{o3}, the largest transient crest prior to the regular wave train, the largest transient trough prior to the regular wave train, and the first regular crest in the wave train, respectively. The initial roll angle and roll velocity were sampled at these points and the results are plotted below.

Initial condition pairs, roll angle and roll velocity, are plotted in Figs. 9-12. Initial conditions that did not lead to capsize are left unfilled. Initial condition pairs that did lead to capsize are filled in. These initial conditions are plotted as global roll angles, that is as referenced to the horizon, not the local wave slope. All the plots have the same scale.

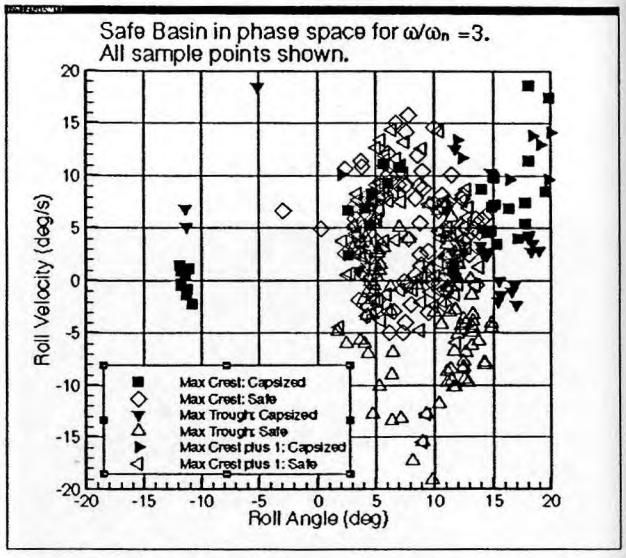

Figure 9: Safe basin with sample points plotted for all phases: Maximum transient crest (t_{o1}), Maximum transient trough (t_{o2}), Maximum transient crest plus one (t_{o3}).

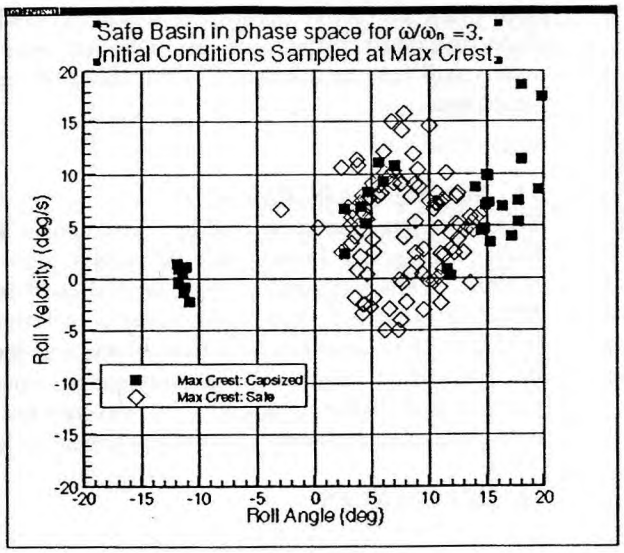

Figure 10: Safe basin from Maximum transient crest sample point (t_{o1})

Figure 9 contains all three initial conditions plotted on one graph. This is done to emphasize the general trends in the capsize and non-capsize data. There appear to be differences in the initial condition pairs when chosen from different starting points, however they all map into the same general vicinity. Figures 10, 11, and 12 contain the same data as figure 9, but are categorized based on whether they are referenced to t_{o1}, the maximum transient crest, t_{o2}, the maximum transient trough, or t_{o3}, the maximum transient crest plus one (i.e. the first regular wave crest). Figures 11 and 12 contain a subset of the runs shown in Fig. 10.

Figure 13 is a comparison plot between the numerical simulation runs and the experimental runs, sampled at the maximum transient crest (Fig. 10). The simulations were run with initial conditions spanning $-20 \leq \varphi \leq 20$ and $-15 \leq d\varphi/dt \leq 15$.

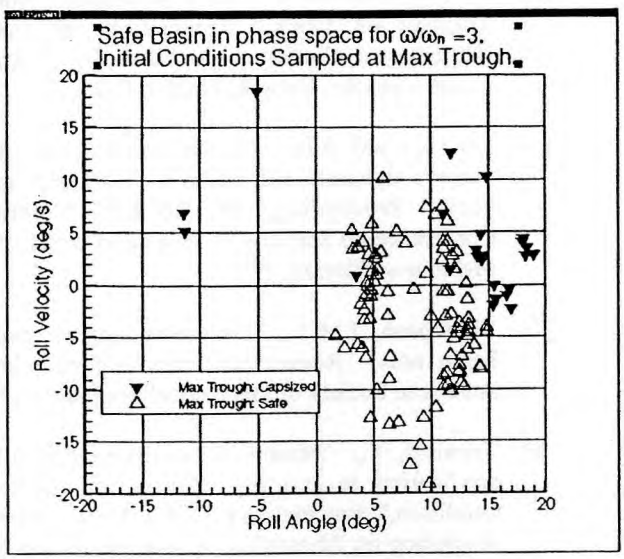

Figure 11: Safe basin from Maximum transient trough sample point (t_{o2})

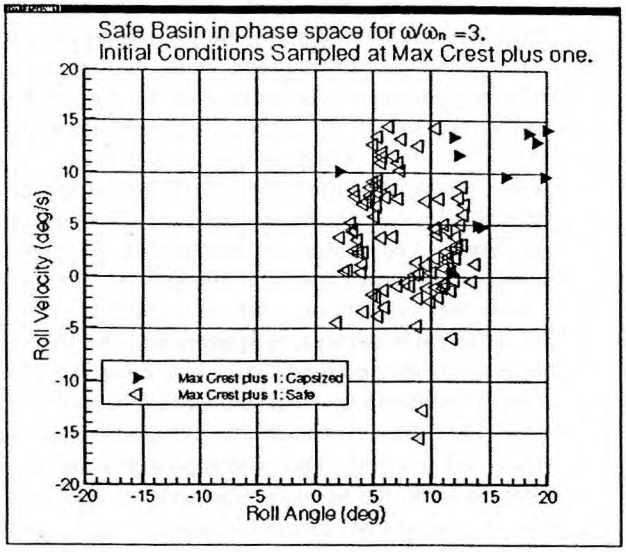

Figure 12: Safe basin from Maximum transient crest plus one (i.e. first regular wave crest) sample point (t_{o3})

White areas within the simulation initial condition boundaries of Fig 13 denote safe or non capsize behaviour, as determined by the integration of Eq.(1). There is significant correlation between the experiments and theory even though the simulations did not match initial conditions for heave and sway and additionally, lack a better dynamic model for water on deck. It is clear that more work is needed in this area to improve the predictions. However, it is also gratifying that the concept of nonlinear systems analysis with various basins of attraction (safe or capsize) [1] [7] seems to capture the physics of capsize.

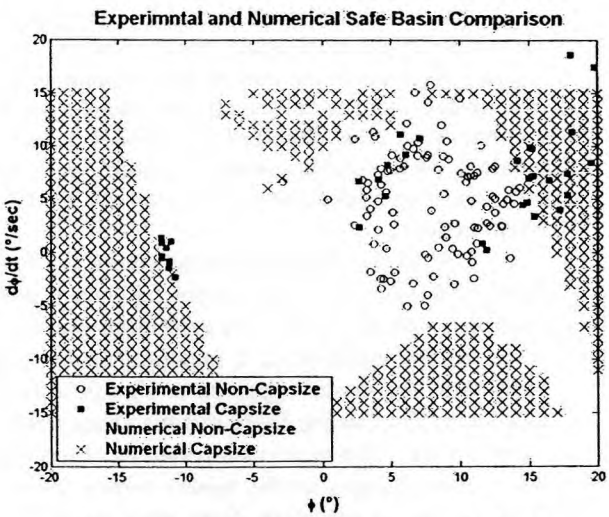

Figure 13: Safe basin plot of numerical and experimental data

10 CONCLUSIONS

The role the initial conditions play in vessel capsize is no doubt an important one. This can be seen where a slight variation in an initial condition can lead to either capsize or non-capsize. In addition, the location where the wave crashes on the deck of the vessel can be significant in

vessel stability assessment. The water on deck clearly introduces another degree of freedom to the problem.

While conducting the experimental runs, it was noticed that there were times when the vessel appeared to be on the verge of capsize, only to be saved by the dynamics of the water on deck. The converse was also true. A situation where the vessel did not appear to be in danger, was exasperated by the next wave crashing down on deck. In order to study this phenomena, the undisturbed wave surface taken from the laser sheet videos was overlaid onto the vessel motion videos. Based on these video records, it appears that the location of the main deck intersection relative to the surface of the wave either continually saved or immediately sank the vessel.

The model was heeled to both port and starboard roll angles and released. Due to damping and the effect of the water on deck, the vessel almost always settled out to port prior to reaching the defined initial condition sample point, t_o. In several cases, the vessel even capsized during the transient wave front. The runs that capsized early were generally those that started heeled to starboard and were released right before the largest transient struck the vessel. During these runs, the model rolled back to port and as the large transient piled water onto the port side of the model, it continued its roll all the way to capsize.

Runs that were released early, tended to settle out to a motion that rolled about 7 to 10 degrees globally to port. Trends in which release times led to which initial conditions, and thus to capsize or not, need to be looked at. Also, quantification of the amount of water on deck and a general location of the "wedge of water's" center of gravity needs to be determined. This should explain the vessels motion settling about a port roll angle between 7 and 10 degrees.

The vessel always capsized into the waves, to port, for these data collection runs. While conducting preliminary tests to determine the incident wave for this experiment, there were several wave height and frequency combinations that capsized the model away from the incident wave finally selected. Future work with these other wave combinations may help clarify the affect of the water on deck.

Due to the different release times, the longitudinal location of the model (distance for the wave maker) at each defined t_o varied greatly. As mentioned previously in the wave determination tests, a variation in the longitudinal position of the model appeared to significantly effect the location of the capsize basin and the characteristics of the capsize wave. This can be addressed by observing how the wave front changes as the model moves down the tank. (This change in the wave front leads to different initial conditions.) However further analysis should be conducted, including running tests starting from the same initial conditions and relative release time but varying the longitudinal release location in the tank.

These experiments and numerical simulations represent a starting point for the development of a practical tool for classifying safe and dangerous dynamic conditions for a specific vessel in a specific loading condition. Completing the above mentioned follow-on analysis and conducting future testing with this and other more complex models will lead to a better understanding of the capsize phenomena.

11 ACKNOWLEDGEMENTS

This paper has been sponsored by the Michigan Sea Grant College Program, Project R/T-32, under grant number NA89AA-D-SG083 Amd #5 from the Office of Sea Grant, National Oceanic and Atmospheric Administration (NOAA), U.S. Department of Commerce, and funds from the State of Michigan. The government is authorized to produce and distribute reprints for government purpose notwithstanding any copyright notation appearing herein.

12 REFERENCES

[1] Soliman and Thompson, 'Transient and steady state analysis of capsize phenomena', Applied Ocean Research, 1991.

[2] Murashige, S. and Aihara, K., "Coexistence of periodic roll motion and chaotic one in a forced flooded ship, International Journal of Bifurcation and Chaos, Vol. 8, No. 3, pp. 619-626, 1998.

[3] Huang, Z.J., Cong, L., Grochowalski, S., and Hsiung, C.C., "Capsize analysis for ships with water shipping on and off the deck," Proceedings of the 22nd Symposium on Naval Hydrodynamics, Washington, DC, 1998.

[4] Huang, Z.J. and Hsiung, C.C., "Nonlinear shallow water flow on deck coupled with ship motion," Proceedings of the 21st Symposium on Naval Hydrodynamics, Trondheim, Norway, 1996a.

[5] Pantazopoulos M. and Adee, B., "An Experimental Investigation of a Vessel Response with Water Trapped on Deck," Proceedings of the Third International Conference on Stability of Ships and Ocean Vehicles, Gdansk, Poland, 1986.

[6] Lee, K. and Adee, B., "Numerical analysis of a vessel's dynamic responses with water trapped on deck," Proceedings of the Fifth International Conference on Stability of Ships and Ocean Vehicles, Melbourne, Florida, 1994.

[7] Thompson, J.M.T., "Designing against capsize in beam seas: Recent advances and new insights," American Society of Mechanical Engineers, 1997.

[8] Takaishi, Y., "Model test on damage stability and application to stability criteria for flooded deck condition," Proceedings of the Third International Workshop on Theoretical Advances in Ship Stability and Practical Impact, Athens, Greece, 1997.

[9] Ishida, S., Murashige, S., Watanabe, I., Ogawa, Y., and Fujiwara, T., "Damage stability with water on deck of a ro-ro passenger ship in waves," Proceedings of the Second Workshop on Stability and Operational Safety of Ships, Osaka, Japan, 1996.

[10] de Kat, J.O., "Dynamics of a ship with partially flooded compartment," Proceedings of the Second Workshop on Stability and Operational Safety of Ships, Osaka, Japan, 1996.

[11] Amagai, K., Ueno, K, and Kimura, N., "Characteristics of roll motion for small fishing boats," Proceedings of the Second Workshop on Stability and Operational Safety of Ships, Osaka, Japan, 1996.

[12] Beck, R. F. and Reed, A., "Modern seakeeping computations for ships", Proceedings 23rd Symposium on Naval Hydrodynamics. 2000.

[13] ISSC, "Extreme hull girder loading", Committee VI.1 report, 14th International Ship and Offshore Structures Congress, Nagasaki, JAPAN, 2000.

[14] Chen, S. L. , Shaw, S. W., Troesch, A. W., "A systematic approach to modeling nonlinear muli-DOF ship motions in regular seas", Journal of Ship Research, Vol. 43, No. 1, 1999.

[15] Beck, R. F. and Troesch, A. W., "Department of Naval Architecture and Marine Engineering student's documentation and users' manual for the computer program SHIPMO.BM", University of Michigan, Ann Arbor, 1990.